

Original Article

Bioactive PLGA/tricalcium phosphate scaffolds incorporating phytomolecule icaritin developed for calvarial defect repair in rat model

Guang-Sen Shi^c, Ying-Ying Li^a, Ya-Ping Luo^a, Jian-Feng Jin^e, Yu-Xin Sun^b, Li-Zhen Zheng^b, Yu-Xiao Lai^d, Long Li^d, Guo-hui Fu^a, Ling Qin^{b,d}, Shi-Hui Chen^{a,b,*}

^a Pathology Center, Shanghai General Hospital/Faculty of Basic Medicine, Shanghai Jiao Tong University School of Medicine, Shanghai, PR China

^b Department of Orthopaedics & Traumatology, The Chinese University of Hong Kong, Hong Kong SAR, China

^c Department of Ophthalmology, Shanghai General Hospital, Shanghai Jiao Tong University School of Medicine, Shanghai, PR China

^d Translational Medicine R&D Center, Shenzhen Institutes of Advanced Technology, Chinese Academy of Sciences, Shenzhen, PR China

^e Department of Biochemistry and Molecular Biology, Hainan Medical University, Haikou, PR China

ARTICLE INFO

Keywords:

Low-temperature rapid-prototyping technology
Composite scaffold
Calvarial bone defects
Icaritin
Osteogenesis
Osteoclastogenesis

ABSTRACT

Background/objectives: For treatment of large bone defects challenging in orthopaedic clinics, bone graft substitutes are commonly used for the majority of surgeons. It would be proposed in the current study that our bioactive scaffolds could additionally serve as a local delivery system for therapeutic small molecule agents capable of providing support to enhance biological bone repair.

Methods: In this study, composite scaffolds made of poly (lactic-co-glycolic acid) (PLGA) and tricalcium phosphate (TCP) named by P/T was fabricated by a low-temperature rapid prototyping technique. For optimizing the scaffolds, the phytomolecule icaritin (ICT) was incorporated into P/T scaffolds called P/T/ICT. The osteogenic efficacies of the two groups of scaffolds were compared in a successfully established calvarial defect model in rats. Bone regeneration was evaluated by X-ray, micro-computerised tomography (micro-CT), and histology at weeks 4 and/or 8 post-implantation. *In vitro* induction of osteogenesis and osteoclastogenesis was established for identification of differentiation potentials evoked by icaritin in primary cultured precursor cells.

Results: The results of radiographies and decalcified histology demonstrated more area and volume fractions of newly formed bone within bone defect sites implanted with P/T/ICT scaffold than that with P/T scaffold. Undecalcified histological results presented more osteoid and mineralized bone tissues, and also more active bone remodeling in P/T/ICT group than that in P/T group. The results of histological staining in osteoclast-like cells and newly formed vessels indicated favorable biocompatibility, rapid bioresorption and more new vessel growth in P/T/ICT scaffolds in contrast to P/T scaffolds. Based on *in vitro* induction, the results presented that icaritin could significantly facilitate osteogenic differentiation, while suppressed adipogenic differentiation. Meanwhile, icaritin demonstrated remarkable inhibition of osteoclastogenic differentiation.

Conclusion: The finding that P/T/ICT composite scaffold can enhance bone regeneration in calvarial bone defects through facilitating effective bone formation and restraining excessive bone resorption.

The translational potential of this article: The osteogenic bioactivity of icaritin facilitated PLGA/TCP/icaritin composite scaffold to exert significant bone regeneration in calvarial defects in rat model. It might form an optimized foundation for potential clinical validation in bone defects application.

Introduction

The reconstruction of cranial defects via facilitating bone regeneration can be a challenging task for craniofacial surgeons that result from trauma, congenital anomaly, or a pathological lesion requires surgical intervention. However, the limitations and clinical problems to autograft

or allograft repair that serves as the most commonly used treatment strategy include allograft resorption, fracture and a limited supply of autografts [1,2]. Currently, many efforts have focused on the development of conductive bone graft substitutes, i.e. biomaterial scaffolds possessing the desirable mechanical property and controlled release of bioactive ingredients for tissue regeneration potentials. Osteopromotive

* Corresponding author. Rm 207, Laohong building, South Chongqing Road 280, Shanghai, PR China.

E-mail address: chensh2015@shsmu.edu.cn (S.-H. Chen).

<https://doi.org/10.1016/j.jot.2020.05.008>

Received 18 December 2019; Received in revised form 18 May 2020; Accepted 29 May 2020

Available online 7 June 2020

2214-031X/© 2020 The Authors. Published by Elsevier (Singapore) Pte Ltd on behalf of Chinese Speaking Orthopaedic Society. This is an open access article under the

CC BY-NC-ND license (<http://creativecommons.org/licenses/by-nc-nd/4.0/>).

growth factors can be incorporated into the porous scaffolds that are then implanted into the bone defects to enhance bone regeneration [3–5]. The issue how to optimize the controlled release of the bioactive component over an extended therapeutic time span and the effect on scaffold degradation kinetics after *in vivo* implantation need to be addressed [6]. Synthetic polymer-based drug delivery systems can potentially optimize drug loading, drug distribution as well as release kinetics to enhance bone tissue regeneration and repair [7,8]. Based on our recent studies on such local delivery systems, biocompatible polylactide-co-glycolide (PLGA) along with ceramic Tri-calcium phosphate (TCP) [9] served as porous composite scaffolds for this study [8].

When deciding on drug to incorporate into the P/T scaffold, Icaritin (ICT), a semisynthesized single phytomolecule formed after intestinal metabolism of Epimedium-derived flavonoids (EF) [10–13], was selected. Our previous study presented that ICT could enhance osteoblasts differentiation, facilitate matrix mineralization, inhibit adipogenesis of mesenchymal stem cells (MSCs) [10,14]. We hypothesized that ICT could be incorporated into porous composite scaffolds (formed as P/T/ICT) with bioactivity preservation and homogeneous distribution ensuring an effective and controlled release.

Our previous *in vitro* studies exactly verified that P/T/ICT scaffold was superior to P/T control scaffold due to preservation of ICT bioactivity and its sustained release from P/T/ICT scaffold, as well as desirable macroscopic and microscopic structure, biocompatibility, degradation rate, and mechanical property of P/T/ICT scaffold [5]. In addition, our *in vivo* studies also presented the optimization in bone regeneration and new vessel formation based on ICT incorporation using our established ulnar bone defect model in rabbits [3,4]. As the inherent differences in tissue microenvironment and mechanical stresses existing between long bone and flat bone will all influence the bone remodeling and mineralization within bone defects, in this study, it is desirable to evaluate the *in vivo* bone regeneration potentials of composite scaffolds in non-load-bearing orthotopic sites in our established rat calvarial defects. New bone formation, new vessel growth, and bone resorption within the bone defects were systematically evaluated.

Materials and methods

Materials

PLGA (LA/GA = 75/25) was purchased from Shandong Institute of Medical Instruments, China. β -TCP was from Beijing Modern Orient Precise Chemical Articles Co., Ltd, China. Icaritin (ICT) was produced by Shanghai U-sea Biotech Co., Ltd, China.

Preparation of P/T scaffolds with ICT incorporation

The composite scaffolds were fabricated using a low-temperature biological-material rapid-prototyping device (3-D printer) (CLRF-2000-II, Tsinghua University, China) [16]. Briefly, PLGA was added with a powder weight to solution volume of 13:100 in organic solvent 1, 4-dioxane. PLGA and TCP powders with a weight ratio of 4:1 were dissolved to form a homogeneous solution, and then ICT powder were supplemented as 0.052:100 (powder weight to solution volume) followed by final homogenization to prepare P/T/ICT scaffolds [17]. The P/T scaffold without ICT supplement was used as the control group. The homogenized paste was then sprayed by a computer-driven nozzle and deposited layer-by-layer based on a pre-designed model [18]. The temperature in the production chamber was -28°C . For finalization, the fabricated scaffolds were freeze-dried until completed vaporization of solvent (Christ Alpha 1–2 LD, UK).

Establishment of calvarial defects in rats

The Animal Experimental Ethics Committee (AEEC) of the corresponding author's institution approved the study protocol (Ref. no: 14/

095/MIS). Eighteen 16-week-old male Sprague Dawley rats (mean \pm standard deviation body weight, 300 ± 20 g) were used to establish calvarial defects model [19]. Under general anesthesia by intraperitoneal injection of ketamine combined with xylazine (v:v = 1:1), the surgical area was followed with a 1 cm cranial skin incision made in an anterior to posterior direction along the midline. Bilateral full-thickness defects of 5 mm in diameter were created in the central area of each parietal bone using a saline-cooled trephine drill. The dura mater was not disturbed. The scaffolds of 2 mm thickness were press-fitted into the defect sites. Post-operative pain relief was managed by Temgesic injections for the first 72 h after surgery. Bilateral defects from eighteen rats were totally 36 defects: 12 defects were selected in each group of three groups, i.e., Defect without any implants, P/T and P/T/ICT implants, the 12 defects in each group were divided into two parts that were for decalcified and undecalcified histology respectively at week 8.

Radiography

High-resolution radiographs of the calvarial defects were obtained immediately after surgery and at weeks 4 and 8 post-surgery using a commercial X-ray machine (Faxitron X-ray Corporation, USA). New bone was quantified both by size and by calculation of the fractional area of the original bone defect occupied by newly formed bone using Adobe photoshop CS5 software. New bone formation within the defects was graded from 1 to 4 according to the amount of fractional new bone area with 0%–25% (score ≤ 1); 25%–50% ($1 < \text{score} \leq 2$); 50%–75% ($2 < \text{score} \leq 3$); and 75%–100% ($3 < \text{score} \leq 4$) [20].

Micro-CT

New bone deposition was also evaluated using three-dimensional micro-computerised tomography (micro-CT) ($\mu\text{CT-40}$, Scanco Medical, Brüttisellen, Switzerland) at 4 and 8 weeks post-surgery [21]. The entire scanned area was set for the calvarial defects together with the surrounding cranial bone and soft tissues in a spatial resolution of $17 \mu\text{m}$ per voxel with a 1024×1024 image matrix. For separating the signals of the mineralized tissue from the background signal, background noise was removed using a low-pass Gaussian filter (Sigma = 1.2, Support = 2) with mineralized tissue being defined at a threshold of 220 [22]. New bone within the calvarial defects was quantified by bone mineral density (BMD), tissue volume (TV), and bone volume (BV).

Hematoxylin and eosin (H&E)

After micro-CT examination at the time-point of 8 weeks, the fixed specimens were decalcified in 10% Ethylenediaminetetraacetic acid (EDTA) for 4 weeks, dehydrated and embedded in paraffin using an Embedding Center (Thermolyne Sybron, Dubuque, IA, USA). Coronal paraffin sections with $5 \mu\text{m}$ thickness of the calvarial defect region were prepared using a microtome (LEICA RM2165, Germany). Sections with H&E staining were digitalized into a microscopic system (LEICA MPS 60, Germany) for descriptive histology and quantitative histomorphometry of new bone regeneration [23]. New bone area and total implant area within the defects were quantified separately using an Image-pro Plus software system (Media Cybernetics, Silver Spring, MD, USA) [23]. Four serial sections from each specimen were used for statistical analysis.

Immunohistochemistry

Immunohistochemical measurement related to osterix (Sp7), osteocalcin (OCN) and von Willebrand factor (vWF) (Abcam), was performed using standard protocols. Positive staining was quantified using an Osteometrics. Specifically, the positive products were quantified and presented as positively stained surface/length of newly formed bone in defects (Pos.Pm). The optical density of positive staining per bone area

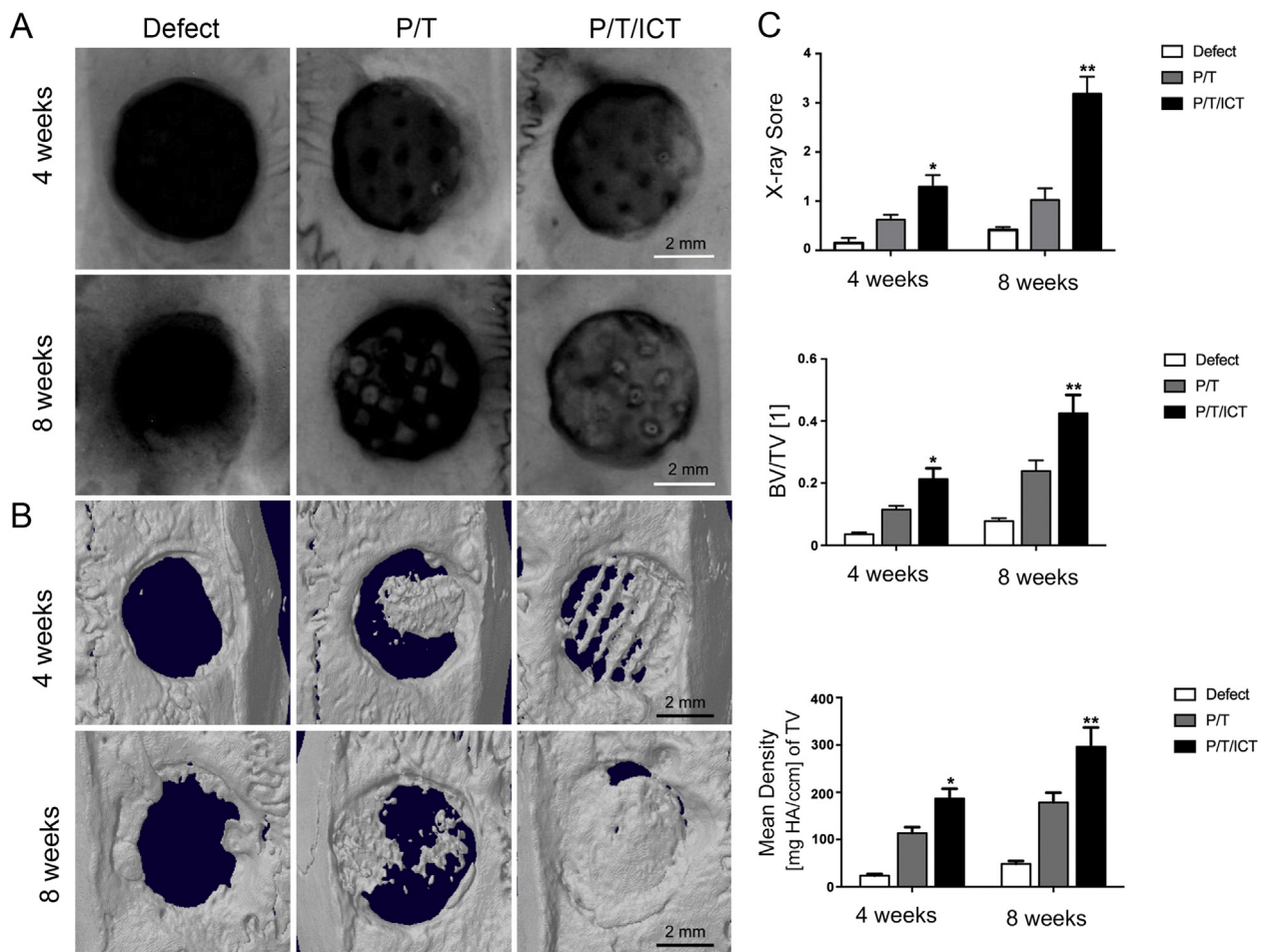


Figure 1. Representative radiographs and micro-CT 3D images at week 4 and 8 post-implantation. (A) X-ray showed fairly homogeneous partial bone regeneration in the P/T group, however, in the P/T/ICT scaffold, almost osseous bridging in defects area was seen along the radial margin extending approximately midway along the defect. Mean percentage of newly formed bone filling the defect regions at 4 and 8 weeks respectively was 15.64% and 25.61% for P/T group, and 32.34% and 79.62% for P/T/ICT group. Radiographic grading scores indicated that there was significantly more bone regeneration in the P/T/ICT group (score: 3.18) compared to the P/T group (score: 1.29) and defect group (score: 0.42) at week 8. (B) Micro-CT demonstrated new bone within the bone defects at weeks 4 and 8. New bone formation as quantified by BMD and BV/TV, was greater in the P/T/ICT group, and less in the P/T group. Bone formation increased further by week 8 in all groups when compared to week 4. N = 6 per group. *p < 0.05, **p < 0.01 compared to P/T group. P/T: PLGA/TCP scaffold; P/T/ICT: PLGA/TCP/icaritin scaffold.

was used to present differences in protein expression for each group.

Tartrate-resistant acid phosphatase (TRAP) staining

TRAP is a well-established marker for osteoclast lineages. A TRAP staining kit (Sigma Diagnostics, St. Louis, MO, USA) was used for osteoclasts identification. Osteoclast number and eroded surface were quantified using the Osteometrics. In selected regions of interest (ROI), parameters were calculated and expressed by N.Oc/SS (the osteoclasts number per scaffolds surface) and Oc.S/SS (the osteoclasts surface per scaffolds surface).

Undecalcified histology

Sequential fluorescence labeling was used to observe dynamic bone remodeling within bone defects [24]. In brief, two fluorescent dyes, xylenol orange and calcein green (Sigma-Aldrich GmbH) were injected subcutaneously into the rats at day 10 and day 3 sequentially before euthanasia. The fixed samples were then dehydrated, and embedded in methyl methacrylate (MMA; Mecck-Schuchardt, OHG, Hohenbrunn, Germany). Mid-coronal sections of bone defect sites were prepared at a thickness of 5 μ m (Leica SM2500E; Leica Instruments, Nussloch, Germany).

Fluorochromes are calcium-seeking molecules that bond to

mineralization fronts at new bone formation sites. Calcein green was positive with green color while xylenol orange was positive with red color. A mixture of calcein green/xylenol orange was positive with green and red color [25]. Goldner's Trichrome staining of MMA sections was used to observe osteoid and mineralized bone tissues. The evaluated histological and cytological parameters were the ratio of osteoblasts surface and bone surface (Ob.S/BS), osteoid surface (Os.Pm), the ratio of osteoid surface and bone surface (Os.S/BS), osteoid area (Os.Ar), mineralizing surface (MS), mineral apposition rate (MAR) and bone formation rate per bone surface (BRF/BS) according to published guidelines for bone histomorphometry [26]. Four serial sections from each specimen were used for statistical analysis.

Primary culture and differentiation of osteoclast

Primary bone marrow cells (BMCs) were harvested from the marrow cavities in tibiae and femora of 12-week-old rats and differentiated into osteoclast precursors using previously described methods [27,28]. Briefly, BMCs were harvested and cultured in Dulbecco's Modified Eagle's Medium containing 10% fetal bovine serum and 1% penicillin-streptomycin (complete medium) for 4 h. Nonadherent BMCs were transferred to new dishes and supplemented with 50 ng/mL of recombinant macrophage colony-stimulating factor (M-CSF) for 3 days. The attached osteoclast precursors were then incubated in complete

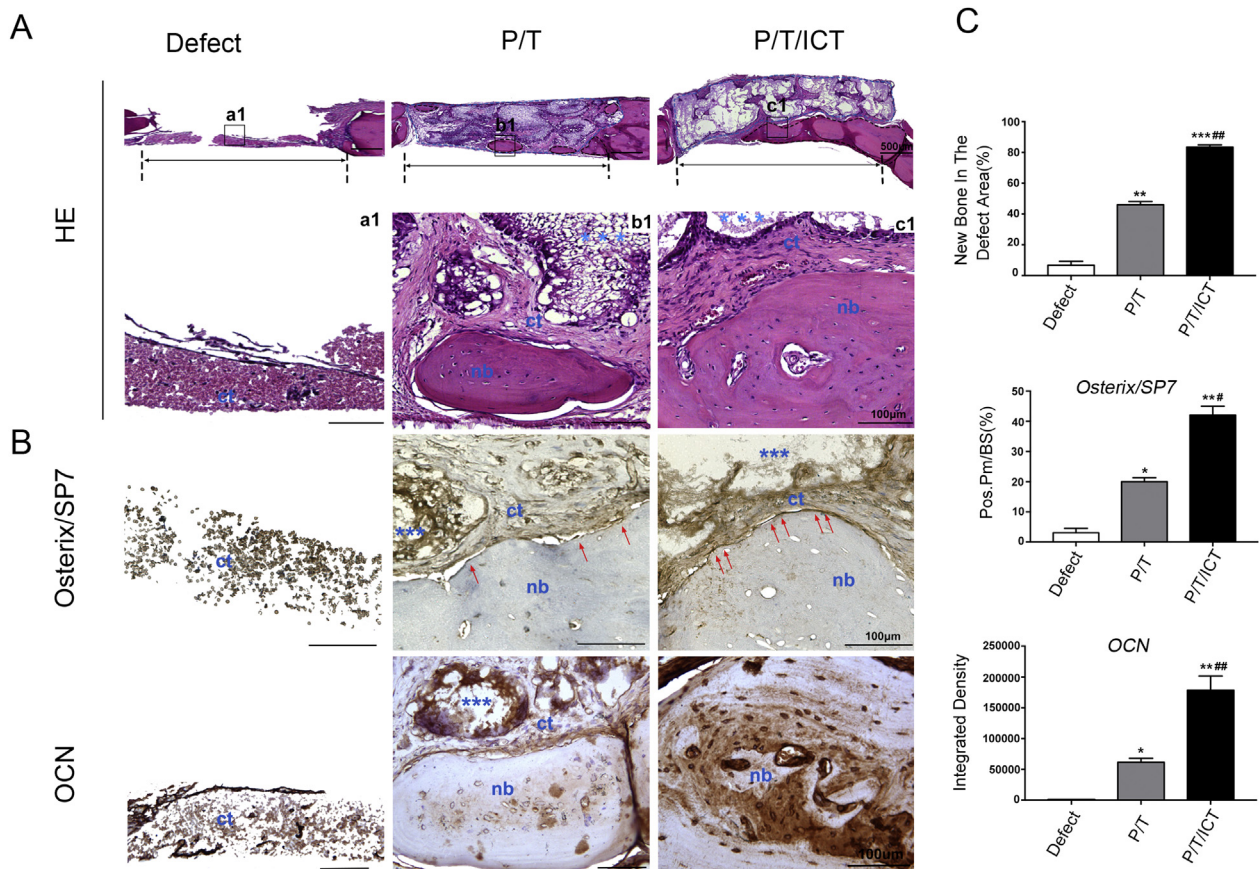


Figure 2. Identification of *in vivo* osteogenic potentials of the scaffolds. (A&C) Compared with defect group without scaffolds implantation, new bone ingrowth into the scaffold pores was evident via H&E staining in scaffolds implanted groups, suggesting good osteoconductivity and biocompatibility of the implanted scaffolds. More newly formed bone within the scaffold was seen in the P/T/ICT to have remodeled towards mature lamellar bone with osteocytes within lacunae embedded in the bone matrix than that showed in the P/T. (B&C) The positive expressions of Sp7 and Osteocalcin were mainly located in the osteoblasts and the bone matrix in new bone tissues within the defects. The results of quantitative analysis presented significantly positive staining in the P/T/ICT in contrast to ones in the P/T. $N = 6$ per group. * $p < 0.05$, ** $p < 0.01$ compared to Defect group; # $p < 0.05$, ## $p < 0.01$ compared to P/T group. P/T: PLGA/TCP scaffold; P/T/ICT: PLGA/TCP/icaritin scaffold.

medium with 30 ng/mL recombinant receptor activator of nuclear factor- κ B ligand (RANKL) and 50 ng/mL recombinant M-CSF [osteoclast-specific medium (OSM)] for 4 days. Then, the differentiated osteoclast-like multinucleated cells (MNCs) were harvested. ICT group cells were given icaritin solution with 10^{-7} M for a total of 6 days. Nonadherent BMCs cultured without OSM or icaritin (blank control, BC) and those cultured with OSM but without icaritin (differentiated control, DC) served as controls ($n = 6$ wells per group).

TRAP staining and osteoassay of resorption pits

A TRAP staining kit was used to measure the activity of MNCs. Briefly, MNCs were fixed and then incubated with the mixture solution provided in the kit for 1 h at 37 °C. Hematoxylin solution was used for cell nucleus positive staining. The number of MNCs was quantified.

For bone absorbing function assay, nonadherent cultured BMCs were seeded onto Corning® 96-well Osteo Assay Surface plates and cultured with OSM as described above. At the end of treatment, MNCs were digested and then removed by PBS wash. The eroded areas were observed and quantified to identify resorption pits by Image J software (National Institutes of Health, Bethesda, USA).

Western blot for TRAP expression in cells

MNCs were harvested and lysed in RIPA buffer (Pierce, Rockford, IL,

USA). Extracted proteins were denatured, separated on sodium dodecyl sulfate–polyacrylamide gels, and then transferred to nitrocellulose membranes with a wet transfer apparatus (Bio-Rad, Hercules, CA, USA). Blots were blocked and incubated with the following primary antibodies: rabbit anti- α -tubulin (Cell Signaling, Danvers, MA, USA) and rabbit anti-TRAP (Abcam). Peroxidase-conjugated, then species-specific, respective secondary antibodies (Abcam) were used for subsequent incubation. Protein bands were visualized by chemiluminescence using a Pierce ECL kit (Thermo Scientific, MA, USA). Image J software was used for densitometric analysis of blots.

In vitro induction of osteogenesis and adipogenesis

Primary cultured bone mesenchymal stem cells (BMSCs) monolayers were treated with osteogenic medium (OM) [5] for 21 days, mineralization of BMSCs was observed and analyzed with Alizarin Red S (Sigma–Aldrich) staining. Adipogenic differentiation was induced in adipogenic medium (AM) [5] for 21 days. BMSCs cultured with OM or AM but without icaritin (induced control, IC) served as control ($n = 6$ wells per group).

Quantitative analysis of mRNA expression of cultured cells

Quantitative real-time polymerase chain reaction was used to quantitatively analyze mRNA expression of osteoblastogenic (*Runx2* and *Sp7*),

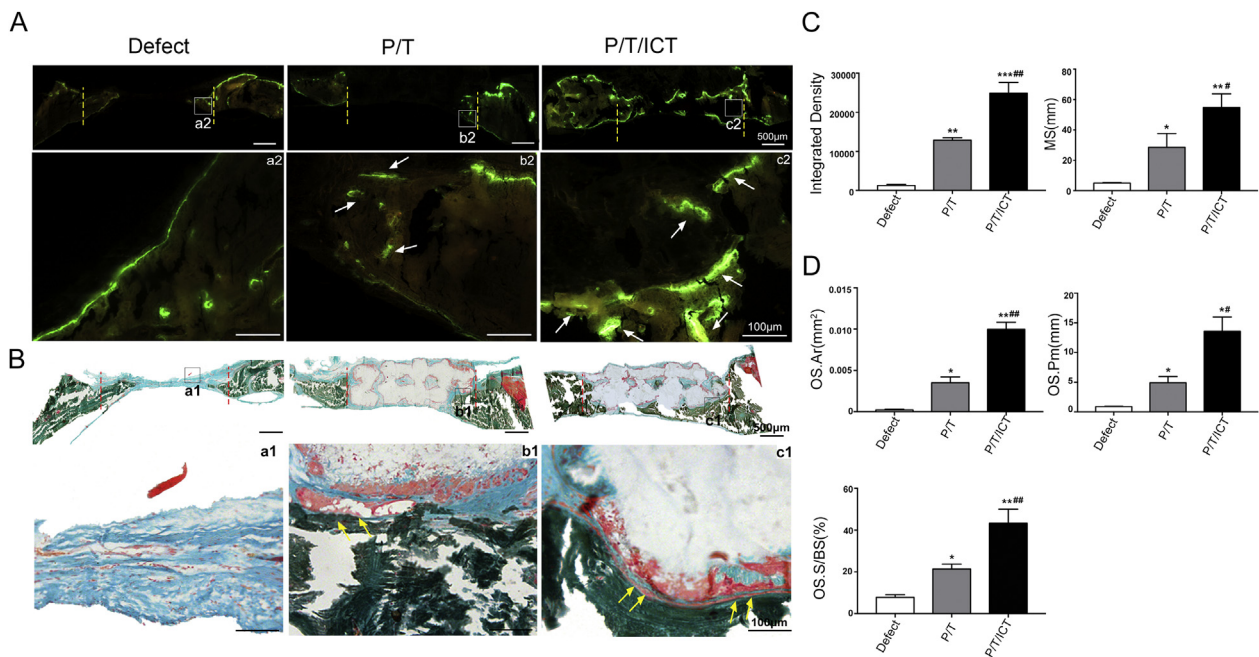


Figure 3. Bone mineralization and bone remodeling in undecalcified histology. (A&C) Fluorescence microscopic images presented more fluorescence deposition in the P/T/ICT group compared to the P/T group, indicating larger isolated new bone islands along the radial margins and within the scaffolds pores. (B&D) Goldner's Trichrome staining showed significantly more new bone formation as dark red staining osteoblasts, red staining osteoid tissue and bluish-green staining mineralized bone tissues in the P/T/ICT group compared to the P/T group. N = 6 per group. * $p < 0.05$, ** $p < 0.01$ compared to Defect group; # $p < 0.05$, ## $p < 0.01$ compared to P/T group. P/T: PLGA/TCP scaffold; P/T/ICT: PLGA/TCP/icaritin scaffold.

osteoclastogenic (*RankL/Opg*), and adipogenic (*Ppar γ 2*) genes. The following cDNA (20 ng) primers were used (Tech Dragon Ltd., N.T., Hong Kong):

Runx2: 5'-CCGATGGGACCGTGGTT-3' (forward) and 5'-CAGCAGAGGCATTCGTAGCT-3' (reverse); *Sp7*: 5'-ATGCCAATGACTACCCACCC-3' (forward) and 5'-ACCACCTAACCAATTGCCCC-3' (reverse);

RankL: 5'-CATGAAACCTCAGGGAGCGT-3' (forward) and 5'-CCCCAAGTACGTCGCATCT-3' (reverse);

Opg: 5'-GCACACGAGTGATGAATGCG-3' (forward) and 5'-AGCAGATTCCGAGCTCCAGG-3' (reverse);

Ppar γ 2: 5'-CGGCGATCTTGACAGGAAAG-3' (forward) and 5'-GCTTCACGGATCGAAACTG-3' (reverse); β -actin: 5'-ATCGTGGGCCCGCTAGGCA-3' (forward) and 5'-TGGCCTTAGGGTTCAGAGGGG-3' (reverse).

Statistical analysis

All quantitative data were presented as mean \pm standard deviation. Differences in bone formation and vessel ingrowth between different scaffolds treatments were analyzed based on one time point by one-way ANOVA test using SPSS version 17.0 (SPSS, Chicago, IL, USA). Statistical significance was set at $p < 0.05$.

Results

New bone formation within the defects

Representative radiographs show the healing process in the bone defects. The results showed fairly homogeneous partial bone regeneration in the P/T group (Fig. 1A). For the P/T/ICT scaffolds, almost osseous bridging in defects area was observed along the radial margin extending approximately midway along the defects. Mean percentage of newly formed bone filling the defect regions at 4 and 8 weeks respectively was 15.64% and 25.61% in the P/T group, and 32.34% and 79.625% in the P/T/ICT groups. Radiographic grading scores (Fig. 1A and C) indicated that there was significantly more bone regeneration in the P/T/ICT group

(score: 3.18) compared to the P/T group (score: 1.29) and the defect group (score: 0.42) at week 8 post-implantation (* $p < 0.05$, ** $p < 0.01$, $n = 6$).

HR-pQCT (Fig. 1B and C) demonstrated newly formed bone within the defects at weeks 4 and 8 after scaffold implantation similar to that showed on radiographs. At 4 weeks post-implantation, more new bone formation as quantified by BMD and BV/TV was presented in the P/T/ICT group than that in the P/T group (* $p < 0.05$, ** $p < 0.01$, $n = 6$). New bone formation increased furthermore by week 8 in all of groups when compared to that in week 4 (* $p < 0.05$).

In decalcified histology, at week 8, new bone ingrowth into the implanted scaffold pores was evident both in the P/T and P/T/ICT groups, suggesting favourable osteoconductivity and biocompatibility of the scaffolds. *In vivo* osteogenesis within the bone defects at week 8 is shown in Fig. 2A. Quantitative analysis (Fig. 2C) shows that at week 8, the P/T/ICT group had more new bone in the defect compared to the P/T group (* $p < 0.05$, ** $p < 0.01$, $n = 6$). The positively stained Sp7 and Osteocalcin were observed in newly formed bone tissues within the defects (Fig. 2B and C). The results presented significantly positive staining in P/T/ICT group in contrast to ones in P/T group (* $p < 0.05$, ** $p < 0.01$, $n = 6$).

As the results of undecalcified histology, at week 8, the P/T/ICT group had more and larger isolated new bone islands along the radial margins and within the scaffolds pores. The newly formed bone within the scaffold had remodeled towards mature lamellar bone with osteocytes within lacunae embedded in the bone matrix. Fluorescence microscopic images showed more fluorescence deposition in the P/T/ICT group compared to the P/T group at week 8 (Fig. 3A and C) (* $p < 0.05$, ** $p < 0.01$, $n = 6$).

Goldner's Trichrome staining successfully differentiated mineralized bone from non-mineralized osteoid. Fig. 3B shows new bone formation as dark red stained cuboidal osteoblasts adsorbed in the macropores of scaffolds lining the surface of red stained osteoid tissue alongside newly bluish-green stained mineralized bone tissue in which mature osteocytes reside. The quantitative results showed significantly more new bone formation, osteoid tissue and mineralized bone tissues in the P/T/ICT

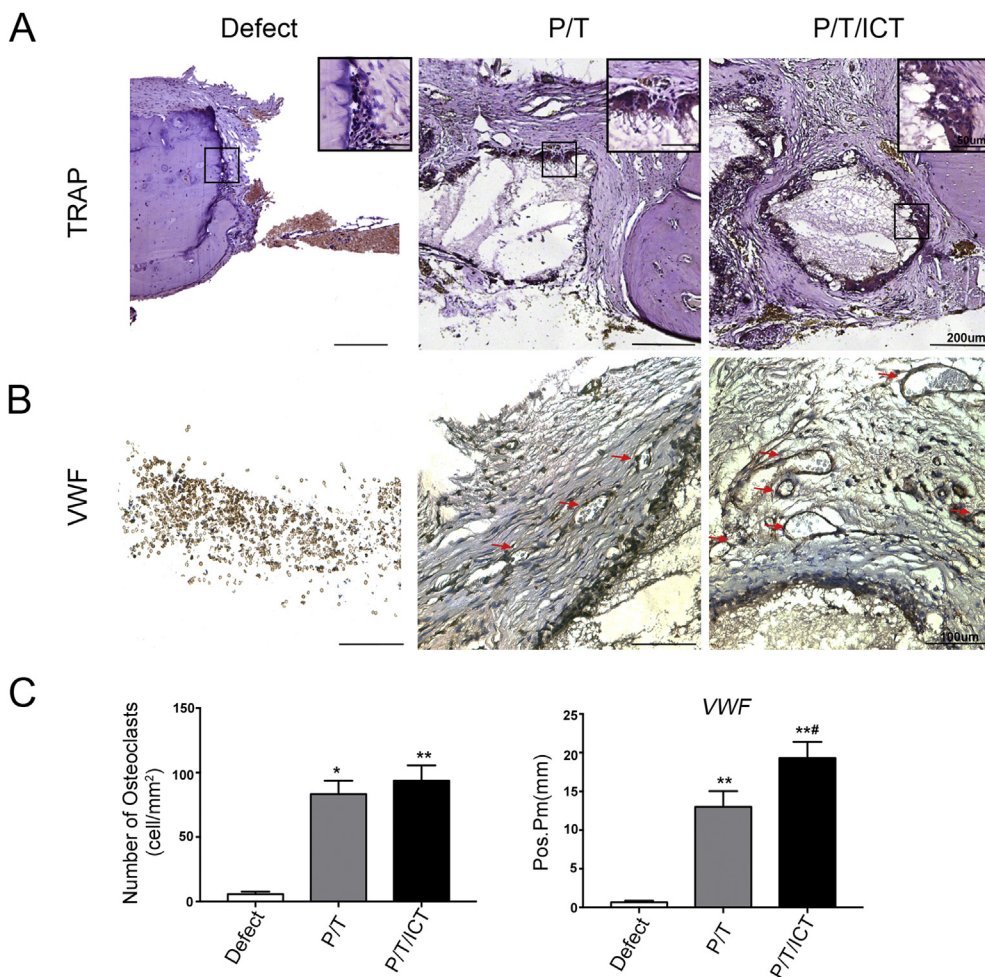


Figure 4. Identification of *in vivo* bone resorption and angiogenesis. (A&C) TRAP-positive staining was detected primarily between stretches of connective tissues attached to the material surface in scaffolds at week 8 post implantation, which indicated favorable biocompatibility and rapid bioresorption of the scaffolds. There was no significant difference of number of multinucleated cells on the scaffolds surface between P/T and P/T/ICT groups. (B&C) Less vWF-positive staining in the bone marrow was observed in the P/T group compared to the P/T/ICT group. N = 6 per group. *p < 0.05, **p < 0.01 compared to Defect group; #p < 0.05, ###p < 0.01 compared to P/T group. P/T: PLGA/TCP scaffold; P/T/ICT: PLGA/TCP/icaritin scaffold.

group compared to the P/T group (Fig. 3B and D) (*p < 0.05, **p < 0.01, n = 6).

Bioresorption and new vessel growth within scaffolds

Positive TRAP-stained multinucleated cells were observed primarily between stretches of connective tissues attached to the surface in scaffolds at week 8 post implantation, which indicated favourable biocompatibility and rapid bioresorption of the scaffolds (Fig. 4A and C). There was no significant difference of number of multinucleated cells on the scaffolds surface between the P/T and P/T/ICT groups (Fig. 4A and C).

Less vWF-positive staining in the bone marrow was observed in the P/T group compared to the P/T/ICT group (Fig. 4B and C).

In vitro osteoclastogenesis inhibition by icaritin

Based on the primary culture of osteoclasts, TRAP staining identified positively-stained MNCs in the DC group. However, the N.Oc was significantly decreased in ICT group compared to the DC group (Fig. 5A). Western blot results of TRAP protein expression in osteoclasts showed a decrease in the ICT group compared to the DC group (Fig. 5B).

For further assessment of osteoclast function, the eroded area of resorption pits was calculated and quantified. The results indicated more resorption pits and larger eroded area in the DC group cells compared to the ICT group (Fig. 5A). Lastly, expression levels of *RankL/Opg* serve an

important role in osteoclast differentiation and maturation. While there was obvious down regulation of these genes in the ICT group compared to the DC group (Fig. 5B).

In vitro induction of osteogenesis and adipogenesis

Alizarin Red S staining showed mineralization with calcium nodule formation (positive staining, dark red) in differentiated BMSCs in the IC group after 21-day osteogenic induction. Interestingly, ICT treatment significantly increased mineralization and calcium nodule formation compared to the IC group (Fig. 5C). Compared to the IC group, no significant difference in *Runx2* mRNA expression was found in ICT treatment group. However, increased *Bglap* expression was indicated in the ICT group compared to the IC (Fig. 5D). In addition, *Pparγ2* expression was significantly lower in the ICT group compared to the IC cells (Fig. 5D).

Discussion

This study was designed to assess the osteogenetic potentials of porous composite scaffolds in an established large-scale calvarial defect model in rats [29]. The concentration of ICT selected for evaluation were optimized by our previous study [3,4]. Based on the quantitative analysis, we found that P/T/ICT scaffolds significantly facilitated bone regeneration compared to P/T scaffolds at both 4 weeks and 8 weeks. The above findings verified our hypothesis that ICT could be incorporated

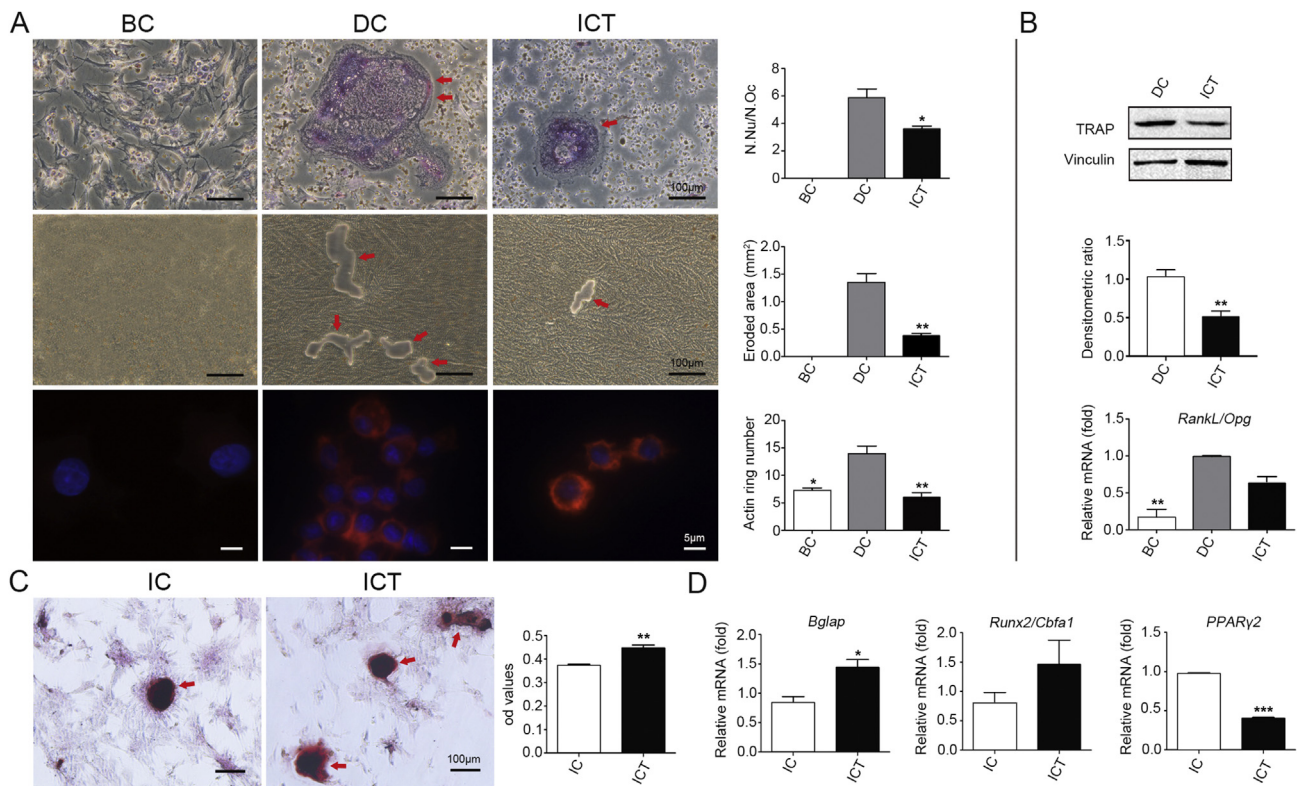


Figure 5. *In vitro* differentiation. (A) TRAP staining identified positively-stained MNCs in the DC group. However, the N.Oc was significantly decreased in ICT group compared to the DC group. The quantitative results indicated smaller eroded area, less resorption pits and actin rings formation in ICT group compared to the DC group. (B) Western blot results presented a decrease expression of TRAP protein in osteoclasts in the ICT group compared to the DC group. There was obvious up regulation of the expression of *RankL/Opg* in the DC group compared to the BC group, while no significant down regulation found in the ICT group compared to the DC group. (C) Alizarin Red S staining showed that ICT treatment significantly increased mineralization and calcium nodule formation compared to the IC group. (D) Compared to the IC group, no significant difference in *Runx2* mRNA expression was found in ICT group. However, increased *Bglap* expression was found in ICT group compared to IC group. In addition, *Ppar γ 2* expression was significantly lower in ICT group compared to IC group. $N = 6$ per group. * $p < 0.05$, ** $p < 0.01$, *** $p < 0.001$ compared to DC or IC group. MNCs: osteoclast-like multinucleated cells; DC: differentiated control; BC: blank control; IC: induced control; ICT: icaritin

into P/T composite scaffolds to promote bone regeneration in calvarial defects in rats. In two published studies from the authors' group [4,5], the biological safety of P/T and P/T/ICT scaffolds was confirmed within a reasonable concentration range [30]. Our previous study also showed that P/T scaffolds loaded with ICT onto the surface of scaffolds but not incorporated into the scaffolds would present less capability of osteogenesis compared to P/T/ICT scaffold although this was slightly better than P/T scaffold, suggesting that ICT promotes bone regeneration through an unique sustainable release or degradation of its efficient components as reported in our *in vitro* [5] and *in vivo* experiments [3].

P/T composite scaffolds facilitated new bone ingrowth

The morphological properties of pore size and porosity of the scaffold are important to bone regeneration and vessel ingrowth [5,31,32]. All of scaffolds fabricated for this study with a ~ 450 μm macropore, ~ 20 μm micropore size and $\sim 70\%$ porosity [4] exactly presented more bone tissue and bone marrow penetrated into the center of scaffolds though the macropores, which showed that all of the scaffolds used may have facilitated bone ingrowth.

Bioabsorbable and biocompatible scaffolds have inherent degradation rates relative to tissue growth rates that results in natural tissue replacement without the long-term complications associated with implants [33]. Bone regeneration was mainly near the cut margins of the

bone defect in implanted scaffolds. This can be explained by the differentiation of BMSCs to form new bone initially adjacent to the surrounding residual bone, where macroporous structure and its progressive degradation may promote BMSCs migration [4].

P/T/ICT composite scaffolds facilitated new bone and new vessel ingrowth

ICT is known as a small phytochemical with its stable phytochemical structure, readily dissolvable without denaturation in organic reagents, and remarkable osteogenic potentials [5,11,13]. P/T/ICT scaffold showed better bone regeneration than P/T scaffold, which might be explained by the preserved bioactivity accompanied by the sustained release of ICT molecules from the incorporated scaffolds [3,14]. These findings are consistent with ones in our *in vitro* study that ICT incorporated scaffolds had better mechanical properties and slower degradation compared to P/T control scaffolds [5]. *In vivo* histological results showed that the scaffold provided good mechanical support up to 8 weeks [34]. Meanwhile, released ICT from the incorporated scaffolds could facilitate BMSCs adhesion, proliferation, migration and differentiation.

In successful bone regeneration, angiogenesis facilitated by growth factors helps supply nutrients and delivers critical biological stimuli for MSCs' osteogenic differentiation [35,36]. The porosity of scaffold can positively affect angiogenesis favoring vascular conduction and growth. In this study, vWF staining of IHC presented that new vessel ingrowth

settled by 8 weeks. ICT incorporated scaffolds showed significantly more blood vessel ingrowth into the pores of the scaffolds during bone regeneration compared to P/T control scaffolds. Although the direct angiogenic stimulatory effect of ICT was not presented in our *in vitro* study, this *in vivo* study indicated an enhanced angiogenesis in ICT incorporated scaffolds that might be regulated indirectly via promoting osteogenesis through increased MSCs recruitment [37]. Sustained release of ICT from the scaffolds could promote MSCs migration and subsequent angiogenesis and osteogenesis. The underlying molecular mechanism together with cell-material matrix interaction should be further investigated.

P/T/ICT composite scaffolds suppressed osteoclasts activities

The biodegradability is basically induced by osteoclastic resorption followed by subsequent new bone formation. A study by Kondo et al. [38] showed that osteoclasts adhere to β -TCP and resorb β -TCP implants continuously from 4 to 56 days after surgery. In this study, TRAP-stained multinucleated cells were observed surrounding either P/T or P/T/ICT scaffold at week 8 post implantation. Interestingly, it was reported that intramuscular osteogenesis using β -TCP and BMP-2 often resulted in a loss of ectopically formed bone [39]. This may also occur due to an imbalance of bone resorption and bone formation, and insufficient numbers of osteoblast progenitor cells in muscular tissue may not be able to overtake the active resorption of implanted β -TCP and form the new bone tissue. The results in this study showed there was not excessive resorption over the replacement with newly formed bone occurred in specimens implanted with P/T or P/T/ICT scaffolds up to 8 weeks post-operation. It implied that the scaffolds had no excessive stimulation of bone resorption and had adequate replenishment of bone formation in bone defect sites. Although there was no significant difference between P/T and P/T/ICT scaffolds, we further clarified the suppressive effects of ICT in osteoclasts activities via inhibiting osteoclasts differentiation or maturation and down-regulating the balance between RANKL and its antagonist OPG as well based on our *in vitro* results. It was explained that ICT possessed recruitment function to osteoclasts during biodegradability and bioresorbability post scaffolds implantation, and then ICT would play an inhibiting role to excessive activities of osteoclasts post implantation in bone defects for more new bone formation. It was reported that rh-BMP-2/ β -TCP could mediate the activation of both osteoclast progenitor cells and mature osteoclasts [40], subsequently leading to excessive resorption of neonatal bone at week 12 post-implantation [40]. So an ideal bone substitute should have proper bioresorbable ability and a balance of resorption and bone formation. Our further study should evaluate the observable inhibitive effects of bone resorption in bone defects post implantation in the final time-point.

Conclusion

P/T scaffolds incorporating ICT significantly enhanced bone formation compared to P/T control scaffold. P/T/ICT composite scaffold is an innovative and ideal bone substitute capable to enhancing bone regeneration but no stimulating excessive bone resorption with potential clinical orthopaedic application.

Funding

This work was supported by Shanghai Natural Science Foundation (18ZR1421800), National Natural Science Foundation of China (No. 51303041), National Natural Science Foundation of China (No. 51573206).

Conflicts and Interest

The authors have no conflicts of interest relevant to this article.

Acknowledgement

This work was supported by Shanghai Natural Science Foundation, China (18ZR1421800), National Natural Science Foundation of China (No. 51303041), National Natural Science Foundation of China (No. 51573206).

References

- [1] Goldberg VM, Stevenson S. Natural history of autografts and allografts. *Clin Orthop Relat Res* 1987;225:7–16.
- [2] Springfield D. Autograft reconstructions. *Orthop Clin N Am* 1996;27(3):483–92.
- [3] Chen SH, Lei M, Xie XH, Zheng LZ, Yao D, Wang XL, et al. PLGA/TCP composite scaffold incorporating bioactive phytomolecule icaritin for enhancement of bone defect repair in rabbits. *Acta Biomater* 2013;9(5):6711–22.
- [4] Chen SH, Zheng LZ, Xie XH, Lei M, Wang XL, Lai YQ, et al. Comparative study of PLGA/TCP scaffolds incorporated or coated with osteogenic growth factors for enhancement of bone regeneration. *J Orthop Transl* 2014;2(2):91–104.
- [5] Chen SH, Wang XL, Xie XH, Zheng LZ, Yao D, Wang DP, et al. Comparative study of osteogenic potential of a composite scaffold incorporating either endogenous bone morphogenetic protein-2 or exogenous phytomolecule icaritin: an *in vitro* efficacy study. *Acta Biomater* 2012;8(8):3128–37.
- [6] Hollister SJ. Porous scaffold design for tissue engineering. *Nat Mater* 2005;4(7):518–24.
- [7] Nair LS, Laurencin CT. Polymers as biomaterials for tissue engineering and controlled drug delivery. *Adv Biochem Eng Biotechnol* 2006;102:47–90.
- [8] Chen S, Lau P, Lei M, Peng J, Tang T, Wang X, et al. Segmental composite porous scaffolds with either osteogenesis or anti-bone resorption properties tested in a rabbit ulna defect model. *Tissue Eng Regen Med* 2017;11(1):34–43.
- [9] Ehrenfried LM, Patel MH, Cameron RE. The effect of tri-calcium phosphate (TCP) addition on the degradation of poly(lactide-co-glycolide) (PLGA). *J Mater Sci Mater Med* 2018;19(1):459–66.
- [10] Qin L, Zhang G, Sheng H, Wang XL, Wang YX, Yeung KW, et al. Phytoestrogenic compounds for prevention of steroid-associated osteonecrosis. *J Musculoskelet Neuronal Interact* 2008;8(1):18–21.
- [11] Wang XL, Xie XH, Zhang G, Chen SH, Yao D, He K, et al. Exogenous phytoestrogenic molecule icaritin incorporated into a porous scaffold for enhancing bone defect repair. *J Orthop Res* 2013;31(1):164–72.
- [12] Zhang G, Qin L, Shi Y. Epimedium-derived phytoestrogen flavonoids exert beneficial effect on preventing bone loss in late postmenopausal women: a 24-month randomized, double-blind and placebo-controlled trial. *J Bone Miner Res* 2007;22(7):1072–9.
- [13] Wang XL, Zhang G, Xie XH, Yao XS, Qin L. Antagonistic estrogen receptor beta signaling required in promoting periosteum bone formation and inhibiting osteoclastic bone resorption by icaritin - a novel synthetic small molecule. *Bone* 2008;43(Suppl):S115.
- [14] Huang J, Yuan L, Wang X, Zhang TL, Wang K. Icaritin and its glycosides enhance osteoblastic, but suppress osteoclastic, differentiation and activity *in vitro*. *Life Sci* 2007;81(10):832–40.
- [15] Kai K, Wang X, Madhukar KS, Qin L, Yan Y, Zhang R, et al. Fabrication of a two-level tumor bone repair biomaterial based on a rapid prototyping technique. *Biofabrication* 2009;1(2):025003.
- [16] Duan B, Wang M. Customized Ca-P/PHBV nanocomposite scaffolds for bone tissue engineering: design, fabrication, surface modification and sustained release of growth factor. *J R Soc Interface* 2010;7(Suppl 5):S615–29.
- [17] Wang X, Yan Y, Pan Y, Xiong Z, Liu H, Cheng J, et al. Generation of three-dimensional hepatocyte/gelatin structures with rapid prototyping system. *Tissue Eng* 2006;12(1):83–90.
- [18] Gu Y, Huang W, Rahaman MN, Day DE. Bone regeneration in rat calvarial defects implanted with fibrous scaffolds composed of a mixture of silicate and borate bioactive glasses. *Acta Biomater* 2013;9(11):9126–36.
- [19] Wan C, He Q, Li G. Allogenic peripheral blood derived mesenchymal stem cells (MSCs) enhance bone regeneration in rabbit tibia critical-sized bone defect model. *J Orthop Res* 2006;24(4):610–8.
- [20] Qin L, Zhang G, Sheng H, Yeung KW, Chan CW, et al. Multiple bioimaging modalities in evaluation of an experimental osteonecrosis induced by a combination of lipopolysaccharide and methylprednisolone. *Bone* 2006;39(4):863–71.
- [21] He YX, Zhang G, Pan XH, Liu Z, Zheng LZ, Chan CW, et al. Impaired bone healing pattern in mice with ovariectomy-induced osteoporosis: a drill-hole defect model. *Bone* 2011;48(6):1388–400.
- [22] Liu G, Sun J, Li Y, Zhou H, Cui L, Liu W, et al. Evaluation of partially demineralized osteoporotic cancellous bone matrix combined with human bone marrow stromal cells for tissue engineering: an *in vitro* and *in vivo* study. *Calcif Tissue Int* 2008;83(3):176–85.
- [23] Qin L, Fok P, Lu H, Shi S, Leng Y, Leung K. Low intensity pulsed ultrasound increases the matrix hardness of the healing tissues at bone-tendon insertion-a partial patellectomy model in rabbits. *Clin Biomech* 2006;21(4):387–94.
- [24] Lu H, Qin L, Fok P, Cheung W, Lee K, Guo X, et al. Low-intensity pulsed ultrasound accelerates bone-tendon junction healing: a partial patellectomy model in rabbits. *Am J Sports Med* 2006;34(8):1287–96.
- [25] Dempster DW, Compston JE, Drezner MK, Glorieux FH, Kanis JA, Malluche H, et al. Standardized nomenclature, symbols, and units for bone histomorphometry: a 2012

- update of the report of the ASBMR Histomorphometry Nomenclature Committee. *J Bone Miner Res* 2013;28(1):2–17.
- [27] Cao HJ, Zheng LZ, Wang N, Wang LY, Li Y, Li D, et al. Src blockage by siRNA inhibits VEGF-induced vascular hyperpermeability and osteoclast activity - an in vitro mechanism study for preventing destructive repair of osteonecrosis. *Bone* 2015;74:58–68.
- [28] Simon D, Derer A, Andes FT, Lezuo P, Bozec A, Schett G, et al. Galectin-3 as a novel regulator of osteoblast-osteoclast interaction and bone homeostasis. *Bone* 2017; 105:35–41.
- [29] Xie XH, Wang XL, Zhang G, He YX, Leng Y, Tang TT, et al. Biofabrication of a PLGA-TCP-based porous bioactive bone substitute with sustained release of icaritin. *J Tissue Eng Regen Med* 2015;9(8):961–72.
- [30] Qin L. Translational medicine in orthopaedics. *J Orthop Transl* 2013;1:3–5.
- [31] Karageorgiou V, Kaplan D. Porosity of 3D biomaterial scaffolds and osteogenesis. *Biomaterials* 2005;26(27):5474–91.
- [32] Cao H, Kuboyama N. A biodegradable porous composite scaffold of PGA/beta-TCP for bone tissue engineering. *Bone* 2010;46(2):386–95.
- [33] Tang J, Wang JL, Xie XH, Zhang P, Lai YX, Li YD. Surface coating reduces degradation rate of magnesium alloy developed for orthopaedic applications. *J Orthop Transl* 2013;1:41–8.
- [34] Powell KM, Skaggs C, Pulliam A, Berman A, Allen MR, Wallace JM. Zoledronate and Raloxifene combination therapy enhances material and mechanical properties of diseased mouse bone. *Bone* 2019;127:199–206.
- [35] Almubarak S, Nethercott H, Freeberg M, Beaudon C, Jha A, Jackson W, et al. Tissue engineering strategies for promoting vascularized bone regeneration. *Bone* 2016; 83:197–209.
- [36] Schipani E, Maes C, Carmeliet G, Semenza GL. Regulation of osteogenesis-angiogenesis coupling by HIFs and VEGF. *J Bone Miner Res* 2009;24(8):1347–53.
- [37] Drushel RF, Pechak DG, Caplan AI. The anatomy, ultrastructure and fluid dynamics of the developing vasculature of the embryonic chick wing bud. *Cell Differ* 1985; 16(1):13–28.
- [38] Cao H, Kuboyama N. A biodegradable porous composite scaffold of PGA/beta-TCP for bone tissue engineering. *Bone* 2010;46(2):386–95.
- [39] Okuda T, Ioku K, Yonezawa I, Minagi H, Kawachi G, Gonda Y, et al. The effect of the microstructure of beta-tricalcium phosphate on the metabolism of subsequently formed bone tissue. *Biomaterials* 2007;28(16):2612–21.
- [40] Ichikawa K, Ohta Y, Mamoto K, Mizokawa S, Minoda Y, Imai Y, et al. Local co-application of zoledronate promotes long-term maintenance of newly formed bone induced by recombinant human bone morphogenetic protein 2. *Biochem Biophys Res Commun* 2016;480(3):314–20.